Microwave Spectrum of the N_2O-SO_2 Dimer: Evidence for Tunneling and an Asymmetric Structure

Rebecca A. Peebles and Robert L. Kuczkowski*

Department of Chemistry, University of Michigan, 930 N. University Ave., Ann Arbor, Michigan 48109-1055

Received: January 18, 2000; In Final Form: March 21, 2000

The microwave spectrum of the nitrous oxide−sulfur dioxide complex has been investigated. The dimer differs from similar complexes of SO_2 with a linear molecule in that it lacks a symmetry plane. A tunneling motion splits the transitions into doublets. This is attributed to an interconversion between mirror-image conformations in which the oxygen atoms on the SO_2 are inequivalent. The rotational constants for the normal species are $A = 6126.9781(15)$ MHz, $B = 1494.537(37)$ MHz, and $C = 1435.474(36)$ MHz for the higher frequency component of the doublets and $A = 5500$ MHz (fixed), $B = 1463.483(23)$ MHz, and $C = 1420.953(23)$ MHz for the lower frequency component. Spectra for four isotopomers in addition to the normal species have been measured, and the dipole moment of the complex has been determined to be 1.212 D. A semiempirical model with atom−atom interaction terms is consistent with an asymmetric equilibrium structure.

Introduction

Recent papers have reported the rotational spectra of three weakly bonded dimers of SO_2 with linear triatomic species.[1−3] The structural conclusions of these three studies are illustrated in Figure 1. The SO_2 straddles the linear molecule in the three dimers. In $OCS-SO_2$ and CS_2-SO_2, the C_2 symmetry axis of the SO_2 is tipped from perpendicular to the C_∞ axis of the linear molecule. This is in qualitative agreement with predictions from a semiempirical model employing atom−atom terms for the electrostatic, dispersion, and repulsion interactions. In CO_2-SO_2, the spectral data was consistent with SO_2 perpendicular to the CO_2, while the semiempirical model predicted a small barrier at this C_{2v} structure.

The goal of this study was to compare the N_2O-SO_2 dimer with the other three SO_2 complexes with linear triatomics. Although N_2O is isoelectronic with CO_2, it sometimes exhibits small structural differences in interactions with the same partner, as reported in recent studies of complexes with H_2O and acetylene.[4−8] We were therefore interested in the structural insights from its rotational spectrum and further intrigued by the semiempirical model which predicted a less symmetric structure (C_1 symmetry) than observed for the other three dimers.

This paper reports on the rotational spectra of the N_2O-SO_2 dimer. As will be shown below, the spectral data are more complex than for the SO_2 complexes with the other three linear molecules. It convincingly demonstrates that the ground state structure resembles the other three complexes but lacks a symmetry plane. Evidence for the reduction in symmetry arises in part from a splitting of the transitions into doublets due to a tunneling motion between mirror image forms. This complication precludes us from determining precise structural parameters at this time, even though several isotopic species have been partially assigned.

* Corresponding author.

Experiment

The spectrum of N_2O-SO_2 in the 5.5−14.5 GHz range was measured using the Balle−Flygare[9] Fourier transform microwave spectrometers at the University of Michigan.[10] The complex was produced by expanding a sample of about 1% N_2O and 1% SO_2 in first run He/Ne (9.5% He, 90.5% Ne) through a modified Bosch fuel injector valve or a General Valve Series 9 nozzle into the Fabry−Perot cavity of the spectrometer. A backing pressure of 2−3 bar was used, and the nozzle was aligned perpendicular to the direction of microwave propagation. This alignment eliminates Doppler doublets on the Michigan spectrometers. An initial range of about 1 GHz was searched by employing an autoscan feature which allows relatively fast scanning of large regions of the spectrum.[11] Many transitions were observed. Mixing experiments in which one component at a time was removed from the sample were used to eliminate those transitions that did not require both sample components. Line widths were about 30 kHz full width at half-maximum, and transition frequencies were reproducible to within 4 kHz. While the strongest transitions had a signal-to-noise ratio in excess of 20 after 10 gas pulses, some of the weaker lines required several thousand gas pulses to reach a reasonable intensity.

Stark effect measurements were performed on lines that required both sample components in order to identify and assign transitions belonging to the desired carrier and to enable calculation of the dipole moment components. These measurements employed a pair of 50 cm × 50 cm parallel steel mesh plates spaced about 30 cm apart and located just outside the Fabry−Perot cavity of the spectrometer. Voltages of up to ±6.5 kV were applied to the plates. The electric field was calibrated by measuring the $J = 1 \leftarrow 0$ transition of OCS at 12 162.98 MHz and assuming a dipole moment of 0.7152 D.[12]

All of the isotopic species were measured with enriched samples, although the strongest $^{34}SO_2$ transitions were visible in natural abundance. The isotopically enriched species that were assigned are $^{15}N_2O-SO_2$, $^{15}N_2O-^{34}SO_2$, $^{15}N_2O-S^{18}O_2$, and

10.1021/jp000236p CCC: $19.00
Published on Web 05/02/2000

TABLE 1: Spectroscopic Constants for N_2O-SO_2 and Isotopomers with Isotopic Substitution in N_2O

	N_2O-SO_2		$^{15}N_2O-SO_2$		$N_2{}^{18}O-SO_2$	
	lower	upper	lower	upper	lower	upper
A/MHz	5500[a]	6126.9781(15)	5500	6070.7640(18)	5500	5942.1522(63)
B/MHz	1463.483(23)	1494.537(37)	1418.535(24)	1446.280(48)	1427.895(61)	1462.01(13)
C/MHz	1420.953(23)	1435.474(36)	1379.852(18)	1397.165(48)	1404.170(26)	1418.24(13)
D_J/kHz	72.2(79)	68.23(3)	64.91(27)	69.58(6)	28.39(94)	69.48(13)
D_{JK}/MHz	−1.381(6)	2.232(19)	−2.320(5)	1.530(25)	−2.320[b]	1.414(66)
d_1/kHz	2.32(62)		5.37(30)		5.37[b]	
d_2/kHz		15.7(22)		40.0(16)		50.3(43)
H_J/kHz	−0.188(15)	−0.167(2)	−0.188[b]	−0.1323(6)	−0.188[b]	−0.142(3)
N[c]	7	10	7	10	4	11
$\Delta\nu_{rms}$/kHz[d]	26.25	1.15	42.84	1.21	97.77	4.11

[a] Fixed, not fitted. [b] Fixed at value from normal or $^{15}N_2O{\cdot}SO_2$ species. [c] Number of lines in fit. [d] $\Delta\nu_{rms} = (\sum(\nu_{obs} - \nu_{calc})^2/N)^{1/2}$.

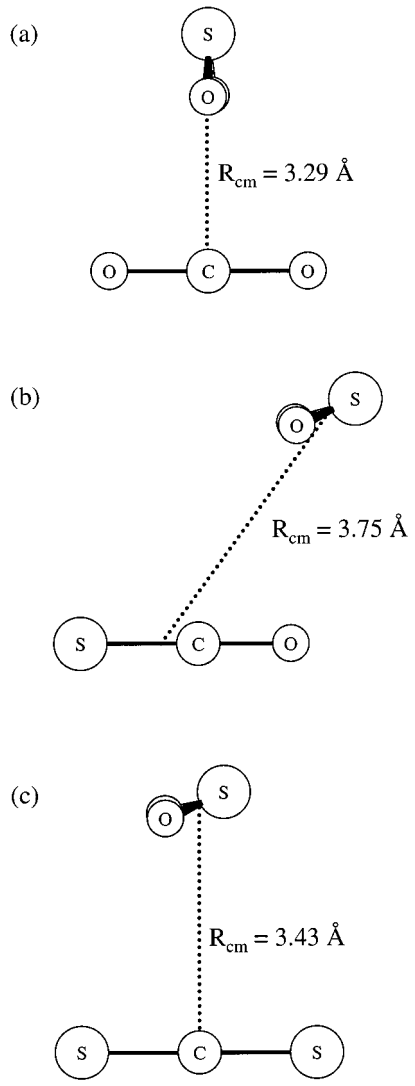

Figure 1. Structures of (a) CO_2-SO_2, (b) $OCS-SO_2$, and (c) CS_2-SO_2. See text for references.

$N_2{}^{18}O-SO_2$. The $^{15}N_2O$ (99% ^{15}N) was obtained from Isotec. The $S^{18}O_2$ (97% ^{18}O) and $^{34}SO_2$ (90% ^{34}S) were obtained from Icon, and the $N_2{}^{18}O$ (48.4% ^{18}O) was obtained from BOC Labs.

Results

A. Spectra. The spectrum of N_2O-SO_2 was observed in the 5.5−14.5 GHz region. Transitions were split from 90 to 200 MHz into doublets. Although dipole moment measurements indicated that all three selection rules operated, predominantly *a*-dipole and some *c*-dipole transitions were assigned. Besides the missing *b*-dipole transitions, some of the *a*-dipole and *c*-dipole transitions were perturbed. The intensity of the *a*-dipole R-branch clusters was unusual for the doublets. For the higher frequency component of the doublet, the $K_a = 0$ and upper $K_a = 1$ transitions were very strong while the lower $K_a = 1$ was weak. This intensity pattern was reversed for the lower doublet component. We have not been able to propose a completely satisfactory explanation for this intensity variation. The weaker intensity of the lower tunneling doublet transitions has been a large factor in our inability to unequivocally confirm the assignments for all the lower frequency components for some isotopic species.

For the normal isotopic species 11 *a*-type and 3 *c*-type transitions were measured for the higher frequency component, and 10 *a*-type transitions were measured for the lower frequency component. Enough Stark splitting measurements for the stronger *a*- and *c*-dipole transitions were made to confirm these assignments along with the frequency fits. The lower $K_a = 1$ transition for the upper frequency component was perturbed, and its intensity was lower. Its Stark effect appeared consistent with the assignment, although its weaker Stark components could not be definitely observed. One possible *c*-type transition for the lower tunneling component of the normal isotopomer was also identified, but failure to identify additional *c*-type transitions made it impossible to confirm this assignment. Similar sets of transitions were measured for the upper tunneling components of the other isotopomers, but assignments of the lower component spectra are relatively uncertain and quite incomplete. Although transitions have been identified that are believed to belong to the lower tunneling component of each species, it has been impossible to identify enough transitions for any of these spectra to unequivocally confirm an assignment. Most lower tunneling doublet transitions are too weak to perform Stark effects on, so this useful tool was eliminated. Another contribution to the difficulty of these assignments was the multitude of lines in some regions where transitions were expected. The close overlap of the upper component of the $^{15}N_2O-{}^{34}SO_2$ species with the lower component of $^{15}N_2O-{}^{32}SO_2$ caused further complication. The strong $^{34}SO_2$ upper component transitions had about the same intensity when measured in natural abundance as was expected for the weak lower tunneling doublets for $^{15}N_2O-{}^{32}SO_2$. Only after a marked increase in intensity was observed upon use of a ^{34}S-enriched sample was this species correctly identified and assigned.

Spectroscopic constants for all of the assigned isotopes are given in Tables 1 and 2, and transition frequencies are given in Tables 3−5. The spectra have been fit to Watson's S-reduction Hamiltonian in the I^r representation. It was necessary to include one P^6 term in order to obtain a fit of reasonable quality. D_K

TABLE 2: Spectroscopic Constants for Isotopomers of $^{15}N_2O-SO_2$ with Isotopic Substitution of SO_2

	$^{15}N_2O-S^{18}O_2$		$^{15}N_2O-^{34}SO_2$	
	lower	upper	lower	upper
A/MHz	5500[a]	5656.5695(99)	5500[a]	6079.7059(53)
B/MHz	1394.46(16)	1426.507(79)	1389.906(20)	1421.64(11)
C/MHz	1333.54(11)	1351.694(78)	1358.757(20)	1376.37(11)
D_J/kHz	64.9 [b]	74.26(13)	39.86(60)	68.09(11)
D_{JK}/MHz	−2.320[b]	2.958(41)	−2.671(9)	1.088(56)
d_1/kHz	5.37[b]		5.37[b]	
d_2/kHz		29.9(26)		54.0(36)
H_J/kHz	−0.188[b]	−0.195(2)	−0.188[b]	−0.131(2)
N[b]	3	10	6	11
$\Delta\nu_{rms}$/kHz[c]	1011	4.18	53.55	3.46

[a] Fixed, not fitted. [b] Fixed at value from normal or $^{15}N_2O\cdot SO_2$ species. [c] Number of lines in fit. [d] $\Delta\nu_{rms} = (\sum(\nu_{obs} - \nu_{calc})^2/N)^{1/2}$.

TABLE 3: Transition Frequencies for N_2O-SO_2 (in MHz)

	N_2O-SO_2 (lower)		N_2O-SO_2 (upper)	
$J'_{K_a'K_c'} - J''_{K_a''K_c''}$	frequency	obs − calc	frequency	obs − calc
$1_{10}-0_{00}$			7616.778	0.001
$2_{12}-1_{11}$	5729.422	−0.020	5822.803	32.989[a]
$2_{02}-1_{01}$	5766.268	0.079[a]	5857.240	−0.002
$2_{11}-1_{10}$	5814.633	−0.020	5907.940	0.000
$2_{11}-1_{01}$			10594.966	−0.014[a]
$3_{13}-2_{12}$	8589.272	0.014	8728.397	48.312[a]
$3_{03}-2_{02}$	8643.923	0.033	8780.154	0.000
$3_{12}-2_{11}$	8717.364	0.013	8857.254	0.001
$3_{12}-2_{02}$			13594.991	−0.001
$4_{14}-3_{13}$	11443.223	0.410[a]	11630.664	66.182[a]
$4_{04}-3_{03}$	11514.703	−0.033	11695.862	0.000
$4_{13}-3_{12}$	11614.319	0.205[a]	11800.605	0.000
$5_{15}-4_{14}$				
$5_{05}-4_{04}$	14375.817	0.007	14601.447	0.069[a]
$5_{14}-4_{13}$			14735.386	0.000

[a] Not included in fit.

and d_1 for the upper set of transitions and D_K and d_2 for the lower set of transitions were poorly determined and thus fixed at zero. It should be noted that for the upper tunneling component there was a very high correlation (1.000 in most cases) between B, C, and D_{JK}. For many of the lower tunneling component fits it was necessary to fix some of the spectroscopic constants at the values from the normal or $^{15}N_2O\cdot SO_2$ species because of the small number of transitions in the fit. The A rotational constant was also fixed for the lower tunneling component, because the lack of c-type transitions prevented determination of this constant. Because of the very small dependence of the a-type transitions in this near prolate top ($\kappa = -0.97$) on the A rotational constant, the value at which A was fixed had only a small effect on the quality of the fit and the values of the other constants. It is assumed that our inability to identify c-type transitions for the lower tunneling doublet spectra is due to these transitions being much weaker than the corresponding higher frequency lines. The only evidence of quadrupole splitting in the spectra was in the c-type transitions. These transitions had two or three strong components, and an estimated center frequency was used in the spectral fitting process. This splitting caused a decrease in the signal intensity which probably added to the difficulty of observing the lower tunneling doublet c-type transitions.

Since each tunneling component could be fit separately without a tunneling splitting correction, we believe that the a- and c-dipole transitions are not tunneling-rotation transitions but pure rotational transitions perturbed by the interaction between tunneling and rotation (so-called Coriolis interactions). The large value of D_{JK} and reversed sign for the two tunneling states is typical of such fits using the Watson Hamiltonian.

One possible b-type transition was observed about 900 MHz above the predicted frequency. A tentative identification as the upper component b-type $J = 1 \leftarrow 0$ transition of the normal species was based on a Stark effect measurement and the fact that a small quadrupole splitting similar to that observed for the c-type $J = 1 \leftarrow 0$ transitions was observed. (The splitting is probably ^{14}N quadrupole related, since the c-dipole transitions for the $^{15}N_2O$ species were unsplit.) Attempts at finding the corresponding $J = 2 \leftarrow 1$ transition were unsuccessful, so we have no conclusive proof that this is indeed a b-type transition. The large perturbation from the predicted frequency is not unexpected, since the direction of the μ_b-component of the dipole moment is presumably reversed by the proposed tunneling motion making this a tunneling−rotation transition.

The observation of all the expected $K = 0$ and $K = 1$ a-dipole transitions for the normal isotope precludes tunneling motions for structures with C_s symmetry, such as rotation about the C_2 axis of SO_2, which would exchange symmetry equivalent oxygen atoms. Such motions would lead to missing levels due to the boson statistics of ^{16}O. The doublet pattern is more indicative of tunneling between mirror image structures with nonequivalent oxygens on the SO_2 and therefore an asymmetric structure. This asymmetry is confirmed by the observation of all three dipole moment components discussed next.

B. Dipole Moment. The dipole moment of the normal isotopomer of N_2O-SO_2 was measured by quantitatively examining the Stark effects of 12 M components from the higher frequency tunneling doublets of seven transitions. Values of $\mu_a = 0.6102(8)$ D, $\mu_b = 0.668(31)$ D, and $\mu_c = 0.806(28)$ D were determined, giving a total dipole moment of 1.212(25) D. The relatively good fit for the three dipole components using the constants in Table 1 and second-order perturbation theory suggests that any tunneling contribution to the b-dipole transitions is less than about 10%. Stark coefficients for the measured transitions are given in Table 6, and the dipole moment components are reported in Table 7 along with predicted values obtained by projecting monomer dipole moments onto the principal axes of four possible experimental structures consistent with the moments of inertia. A discussion of these structures in relation to the experimental dipole moment will be given later in this paper. The presence of all three dipole components indicates a nonsymmetric structure.

C. Structure. As pointed out above, the presence of all the $K_a = 0,1$ a-dipole transitions for both tunneling components, and all three dipole components contributing to the Stark splittings, is consistent with a structure which lacks a symmetry plane. In order to derive more detailed structure information, we have considered whether the rotational constants obtained from fitting the spectra are useful or perhaps too contaminated by tunneling motions to be helpful. It appears that the constants are useful although sufficiently contaminated by rotation−tunneling interaction effects to obscure a precise or even unique structural determination.

Using constants from the upper tunneling component, 14 rotational constants of N_2O-SO_2 are available to determine a structure. (I_c from $^{15}N_2O-S^{18}O_2$ was eliminated, because it fit poorly compared to the other moments of inertia.) Five parameters are required to define the structure for an asymmetric dimer involving a linear molecule, if the monomer structures are assumed to be unchanged upon complexation ($R_{N-O} = 1.185$ Å, $R_{N-N} = 1.128$ Å, $R_{S-O} = 1.431$ Å, and $\theta_{O-S-O} = 119.3°$[13]). The parameters chosen are illustrated in Figure 2. They include

TABLE 4: Transition Frequencies for N_2O-SO_2 Isotopomers with Substitution on N_2O Only (in MHz)

	$^{15}N_2O-SO_2$ (lower)		$^{15}N_2O-SO_2$ (upper)		$N_2{}^{18}O-SO_2$ (lower)		$N_2{}^{18}O-SO_2$ (upper)	
$J'_{K_a'K_c'} - J''_{K_a''K_c''}$	frequency	obs − calc	frequency	obs − calc	frequency	obs − calc	frequency	obs − calc
$1_{10}-0_{00}$			7513.705	0.000			7401.054	−0.006
$2_{12}-1_{11}$	5565.307	0.226[a]	5659.137	29.736[a]	5648.462	−0.102		
$2_{02}-1_{01}$	5594.354	−0.028	5684.244	−0.002			5757.932	0.004
$2_{11}-1_{10}$	5643.093	0.302[a]	5727.631	0.000			5796.367	−0.004
$2_{11}-1_{01}$			10398.170	0.000			10317.467	0.008
$3_{13}-2_{12}$	8343.024	0.017	8484.458	44.916[a]	8470.648	0.117	8604.859	46.156[a]
$3_{03}-2_{02}$	8386.713	−0.050	8521.059	0.002	8496.179	3.754[a]	8631.748	−0.003
$3_{12}-2_{11}$	8460.257	0.041	8586.848	0.000			8689.991	−0.001
$3_{12}-2_{02}$			13300.772	0.000			13249.520	−0.002
$4_{14}-3_{13}$	11114.783	−0.232[a]	11305.571	61.572[a]	11289.299	−0.037	11468.537	65.594[a]
$4_{04}-3_{03}$	11173.030	0.052	11351.218	−0.001	11318.749	0.000	11499.112	0.001
$4_{13}-3_{12}$	11272.461	−0.030	11400.224	0.006[a]			11577.784	0.002
$5_{15}-4_{14}$	13878.488	−0.011			14102.301	−0.990[a]		
$5_{05}-4_{04}$			14172.060	0.000			14357.366	0.000
$5_{14}-4_{13}$			14285.233	0.000			14457.184	0.000

[a] Not included in fit.

TABLE 5: Transition Frequencies for $^{15}N_2O-SO_2$ Isotopomers with Substitution on SO_2 (in MHz)

	$^{15}N_2O-{}^{34}SO_2$ (lower)		$^{15}N_2O-{}^{34}SO_2$ (upper)		$^{15}N_2O-S^{18}O_2$ (lower)		$^{15}N_2O-S^{18}O_2$ (upper)	
$J'_{K_a'K_c'} - J''_{K_a''K_c''}$	frequency	obs − calc	frequency	obs − calc	frequency	obs − calc	frequency	obs − calc
$1_{10}-0_{00}$			7498.897	0.001			7076.934[a]	0.071[a]
$2_{12}-1_{11}$								
$2_{02}-1_{01}$			5593.487	0.001			5552.995	−0.003
$2_{11}-1_{10}$			5634.735	0.005			5616.971	0.003
$2_{11}-1_{01}$			10335.889	0.000			9915.934	0.006
$3_{13}-2_{12}$	8209.988	−0.024	8356.687	44.820[a]	8097.268	−0.993	8244.266	48.537[a]
$3_{03}-2_{02}$	8240.765	0.077	8385.156	−0.006	8185.836	11.810[a]	8322.315	−0.005
$3_{12}-2_{11}$	8304.566	−0.054	8447.618	−0.004	8282.189	0.006	8420.115	0.002
$3_{12}-2_{02}$			13190.024	−0.002			12783.037	−0.006
$4_{14}-3_{13}$	10940.625	0.018	11133.493	59.466[a]	10788.972	0.740	10982.507	65.061[a]
$4_{04}-3_{03}$	10981.417	−0.058	11170.493	0.004	10900.559	13.079[a]	11082.591	0.003
$4_{13}-3_{12}$	11067.991	0.040	11254.808	0.003			11216.366	0.003
$5_{15}-4_{14}$	13667.723	2.544[a]			13477.409	8.106[a]		
$5_{05}-4_{04}$			13946.900	−0.001			13830.072	−0.001
$5_{14}-4_{13}$			14053.796	−0.001			14002.589	−0.001

[a] Not included in fit.

TABLE 6: Stark Coefficients for the N_2O-SO_2 Upper Tunneling Doublet

$J'_{K_a'K_c'} - J''_{K_a''K_c''}$	M	$\Delta\nu/E^2$ [a]	obs − calc[a]
$2_{02}-1_{01}$	1	0.2713	0.0078
$2_{11}-1_{10}$	1	−3.7708	0.0007
$3_{03}-2_{02}$	0	−0.0938	0.0031
	1	−0.0353	0.0009
	2	0.1445	−0.0016
$3_{12}-2_{11}$	1	−0.1372	−0.0030
	2	−0.5305	−0.0061
$4_{04}-3_{03}$	0	−0.0193	−0.0012
	3	0.1038	−0.0070
$4_{13}-3_{12}$	2	−0.0861	−0.0015
	3	−0.1510	0.0076
$5_{05}-4_{04}$	4	0.0854	−0.0054

[a] Units of 10^{-4} MHz cm^2/V^2. Calculated Stark coefficients were obtained using the constants in Table 1 and the experimental dipole components in Table 7.

TABLE 7: Experimental and Predicted[a] Dipole Moment Components for N_2O-SO_2

	expt	structure I projections	structure II projections	structure III projections	structure IV projections
μ_a/D	0.6102(8)	1.456	1.458	1.450	1.441
μ_b/D	0.668(31)	0.333	0.265	0.356	0.210
μ_c/D	0.806(28)	0.314	0.381	0.641	0.722
μ_{total}/D	1.212(25)	1.526	1.529	1.625	1.625

[a] Obtained by projecting the dipole moments of N_2O and SO_2 on the principal axes.

the distance between the centers of mass of the two monomers (R_{cm}), the angle between R_{cm} and the N_2O axis (θ_{5-4-2}), and the angle between the symmetry axis of SO_2 and R_{cm} (θ_{6-5-4}). The rotation of the S6−M5 axis out of the M5−M4−N2 plane is given by $\varphi_{6-5-4-2}$, and the rotation of the SO_2 plane relative to the S6−M5−M4 plane is given by $\varphi_{7-6-5-4}$. The signs of the dihedral angles are consistent with the convention in ref 14.

Least-squares fitting of the moments of inertia led to four possible dimer structures which are illustrated in Figure 3, and the parameters are given in Table 8. Structures I and II are quite similar, with the sulfur end of the SO_2 above the oxygen end of the N_2O. The sulfur atom is rotated slightly out of the M5−M4−N2 plane, and the plane of the SO_2 molecule is tilted so one oxygen points slightly down toward the N_2O and the other tips up away from it. Structures III and IV have a similar tilting and twisting of the SO_2 molecule, but the overall alignment tips the sulfur end of SO_2 farther away from the oxygen end of N_2O. The standard deviations of the inertial fits favor structure II slightly over structure I. Structures III and IV seem a little less likely both because of slightly poorer inertial fits and the seemingly less favorable electrostatic interactions when the oxygens of SO_2 point more toward the oxygen end of N_2O.

Four inertial fits of similar quality arise because the signs of the atom coordinates are ambiguous due to their quadratic dependence on the inertial moments. This ambiguity along with

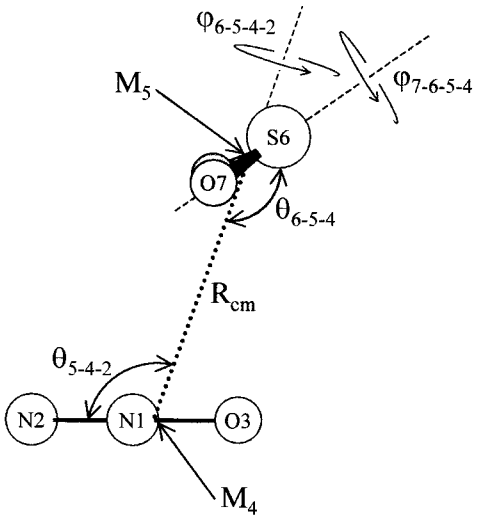

Figure 2. Parameters used to define the structure of N_2O-SO_2. M4 and M5 are the centers of mass of N_2O and SO_2, respectively.

contamination of the moments due to the tunneling motion and other large-amplitude vibrations allows for shifts of atoms across axes (sign changes) with other compensating adjustments in the monomer position resulting in multiple least-squares inertial fits of similar quality. Often one can eliminate some of these structures by comparing their coordinates with a more direct calculation of them using Kraitchman's substitution equations[15] which normally reduces vibrational contamination effects. A partial Kraitchman substitution structure could be obtained due to the assignment of the $N_2{}^{18}O-SO_2$ and $^{15}N_2O-{}^{34}SO_2$ species. Unfortunately, the calculation led to imaginary values for the *b*-coordinates of both O3 and S6. This complication, presumably due to the large-amplitude vibrational motions in the dimer, made a comparison with the four inertial fit structures inconclusive. The absolute values of the substitution coordinates are given in Table 9 along with the principal axis coordinates for the four inertial fit structures. The S6 Kraitchman coordinates vary from structure to structure, because they were determined by using the $^{15}N_2O-{}^{32}SO_2$ species as the parent molecule and then transformed into the principal axis system of $^{14}N_2O-{}^{32}SO_2$. The transformation matrix to carry out this axis system conversion varies slightly depending on the dimer structure used to calculate it. The *a*-coordinates determined for both atoms are in good agreement with the four inertial fit structures, with the closest agreement for structure IV, considering both atoms. The *c*-coordinate of O3 from the Kraitchman calculation agrees relatively well with all four configurations, with structures I and II having the closest value, but agreement for S6 is fairly poor. Only structures III and IV agree at all well with the S6 *c*-coordinate, and structures I and II have very poor agreement with this value. Given the large-amplitude motions present in the complex, the poor agreement between inertial and substitution coordinates is not surprising.

The dipole moment components predicted for the four structures by projecting the dipole moments of the monomers on the complex inertial axes are given in Table 7. The comparison with the experimental values is poor for all the components except μ_c for structures III and IV. The dipole data, like the Kraitchman calculations and inertial fits, is basically inconclusive in distinguishing between the four inertial structures. A combination of polarization effects and vibrational averaging effects on both the dipole components and the inertial structure determinations are the likely origin of the ambiguous results.

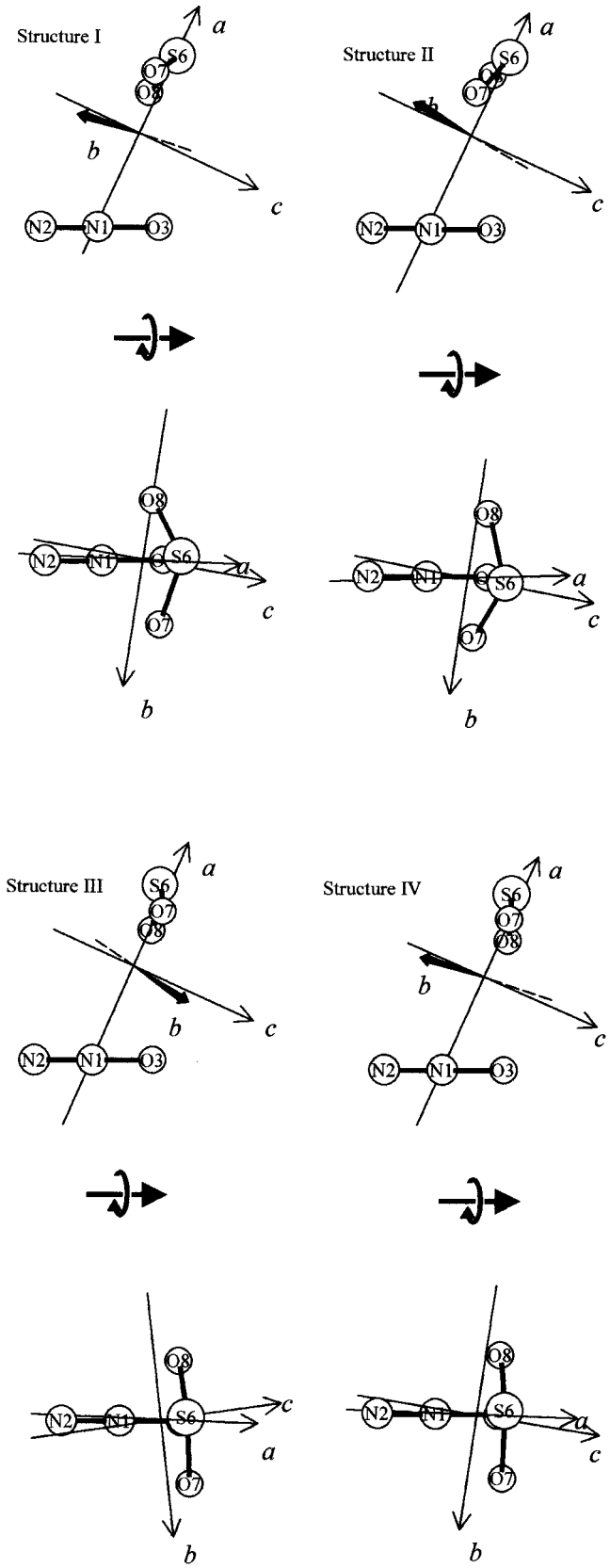

Figure 3. Four structures for N_2O-SO_2 obtained from least-squares fitting of the moments of inertia. In the top view, a plane containing N2 and the centers of mass of both monomers is parallel to the plane of the page. A rotation of 90° about the arrow gives the bottom view in which the N2−M4−M5 plane is perpendicular to the plane of the page.

D. Semiempirical Calculations. The ORIENT[16] semiempirical model was used as a tool for predicting the N_2O-

TABLE 8: Structural Parameters for the Four Inertial Fits[a]

	structure I	structure II	structure III	structure IV	ORIENT
R_{cm}/Å	3.3306(6)	3.3306(6)	3.3306(7)	3.3306(7)	3.618
θ_{5-4-2}/deg	111.2(10)	111.1(10)	111.6(12)	111.7(12)	118.6
θ_{6-5-4}/deg	156.6(51)	156.9(49)	161.3(54)	160.3(58)	101.3
$\varphi_{6-5-4-2}$/deg[b]	−158.3(57)	153.2(66)	−26.2(96)	−30.0(99)	131.4
$\varphi_{7-6-5-4}$/deg[b]	−115.0(59)	−65.2(57)	−119.5(97)	−119.1(87)	122.8
s.d.[c]	0.274	0.267	0.294	0.296	

[a] See Figure 2 for atom numbering scheme. [b] The signs of the dihedral angles are consistent with the definition in ref 14. [c] Standard deviation of the fit in amu Å^2.

TABLE 9: Principal Axis Coordinates for the Four Possible Structures (I, II, III, and IV)[a]

	a				*b*				*c*			
	I	II	III	IV	I	II	III	IV	I	II	III	IV
N1	−1.9989	−1.9989	−2.0000	−2.0002	0.0438	−0.0612	0.0536	0.0478	0.0609	0.0482	0.0137	0.0230
N2	−2.4693	−2.4702	−2.4606	−2.4603	0.2235	0.1061	−0.0716	0.2069	−0.9484	−0.9635	−1.0083	−0.9945
O3	−1.5047	−1.5033	−1.5161	−1.5168	−0.1449	−0.2322	0.1851	−0.1194	1.1213	1.1110	1.0874	1.0920
		[1.525]				[0][b]				[1.210]		
M4	−1.9690	−1.9687	−1.9707	−1.9709	0.0324	−0.0715	0.0615	0.0376	0.1252	0.1126	0.0788	0.0878
M5	1.3545	1.3543	1.3557	1.3558	−0.0223	0.0492	−0.0423	−0.0259	−0.0861	−0.0774	−0.0542	−0.0604
S6	1.6922	1.6923	1.6917	1.6898	−0.1018	0.1028	−0.1174	−0.0775	0.0153	0.0388	−0.1641	−0.1885
	[1.680]	[1.680]	[1.686]	[1.686]		[0][b]			[0.359]	[0.360]	[0.349]	[0.349]
O7	1.2540	0.7776	1.2478	1.2528	1.2596	1.1994	1.2399	1.2337	−0.0335	−0.0538	−0.0716	0.1823
O8	0.7801	1.2554	0.7919	0.7913	−1.1452	−1.2081	−1.1746	−1.1823	−0.3414	−0.3334	0.1830	−0.0469

[a] Absolute values of Kraitchman substitution coordinates are given in brackets. [b] These are set at zero; Kraitchman's equations gave imaginary values.

TABLE 10: Distributed Multipole Moments for N_2O[a]

atom	z[b]	Q_{00}	Q_{10}	Q_{20}	Q_{30}	Q_{40}
N	0.000	1.351 99	0.178 42	0.070 26	−0.374 72	0.254 30
N	−2.132	0.476 21	0.661 66	0.228 73	0.195 97	0.087 04
O	2.239	−0.125 95	−0.397 04	0.901 24	−0.134 32	0.020 99
BC1[c]	−1.066	−1.137 77	−0.004 14	0.589 64	0.130 92	0.441 28
BC2[c]	1.121	−0.564 48	0.031 24	0.198 86	0.032 67	−0.057 22

[a] All quantities are in atomic units. [b] z refers to the z-coordinate of the atom. [c] BC1 and BC2 refer to the midpoints of the bonds.

SO_2 structure. As discussed in refs 2 and 3, this program has also been employed for analyzing the CO_2-SO_2, $OCS-SO_2$, and CS_2-SO_2 structures. The ORIENT model uses distributed multipole moments (DMMs) to model the electrostatic part of the intermolecular interaction potential and terms of the form given in eq 1:

$$U_{\exp-6} = \sum_{i,j} K \exp[-\alpha_{ij}(R_{ij} - \rho_{ij})] - \frac{C_6^{ij}}{R_{ij}^6} \qquad (1)$$

to model the dispersion and repulsion interactions. A detailed explanation of the terms of this equation can be found in the previous papers[2,3] or in Stone's recent book on intermolecular forces.[17] Induction effects are usually not included in the calculation, but point polarizabilities placed on the molecules or distributed polarizabilities calculated with an ab initio program can be used to account for them. The DMMs were calculated using the CADPAC suite of programs[18] with a TZ2P basis set from the CADPAC library, and they are listed in Tables 10 and 11. Moments were calculated at bond centers as well as atom centers, since this has been shown to better reproduce experimental results for other SO_2 complexes.[2,3] Values of the α, ρ, and C_6 terms in eq 1 have been calculated by Mirsky[19] and are listed in Table 11.2 of ref 17.

Although a structure with C_1 symmetry was predicted for each of the three other SO_2 complexes, C_s structures were also predicted for each of them. Except in the case of CO_2, the experimental data was consistent with the predicted structures

TABLE 11: Distributed Multipole Moments for SO_2[a]

	S	O	O	BC1	BC2
Q_{00}	1.908 11	−0.081 98	−0.081 98	−0.872 08	−0.872 08
Q_{11c}	0.000 00	−0.428 45	0.428 45	−0.199 28	0.199 28
Q_{11s}	−1.783 74	0.417 97	0.417 97	0.167 83	0.167 83
Q_{20}	−0.202 67	−0.250 03	−0.250 03	−0.664 04	−0.664 04
Q_{22c}	1.321 20	0.356 91	0.356 91	−0.243 56	−0.243 56
Q_{22s}	0.000 00	−0.857 11	0.857 11	−0.698 49	0.698 49
Q_{31c}	0.000 00	0.438 57	−0.438 57	−0.374 98	0.374 98
Q_{31s}	0.194 47	−0.329 47	−0.329 47	0.127 72	0.127 72
Q_{33c}	0.000 00	0.302 26	−0.302 26	−0.004 23	0.004 23
Q_{33s}	0.432 77	0.607 14	0.607 14	−0.465 19	−0.465 19
Q_{40}	0.271 40	0.268 53	0.268 53	0.089 71	0.089 71
Q_{42c}	−0.197 08	−0.089 80	−0.089 80	0.093 19	0.093 19
Q_{42s}	0.000 00	0.385 57	−0.385 57	0.455 09	−0.455 09
Q_{44c}	−0.422 92	−0.467 65	−0.467 65	−0.631 53	−0.631 53
Q_{44s}	0.000 00	−0.209 26	0.209 26	−0.122 04	0.122 04

[a] The coordinates of SO_2 are x(S) = 0.000 00, y(S) = 0.000 00; x(O) = ±2.333 28, y(O) = −1.366 19; x(BC) = ±1.169 62, y(BC) = −0.683 24. All quantities are in atomic units.

of higher symmetry. The highly symmetric C_{2v} structure consistent with the spectrum for $CO_2 \cdot SO_2$ could not be reproduced with the ORIENT program, except as a transition state. When the model was applied to the N_2O-SO_2 system, the only structure that could be obtained was one with C_1 symmetry (see Figure 4), similar to those obtained for the previous three complexes. The C_s structure was found only as a "solution of wrong index" (a saddle point or transition state on the potential energy surface), when it appeared that the structure optimization was converging, but the program stepped away from the structure, since it was not a minimum on the potential energy surface. This second structure was 0.0002 E_h (44 cm^{-1}) higher in energy than the global minimum.

Of the four structures whose parameters are given in Table 8, structures I and II most closely resemble the results of the ORIENT calculation. It should be noted, however, that this resemblance is purely qualitative. While the computation predicts that one S−O bond will be nearly parallel to the N−O bond, the experimental results give a structure where the SO_2 symmetry axis is more nearly coplanar to N_2O. Structural

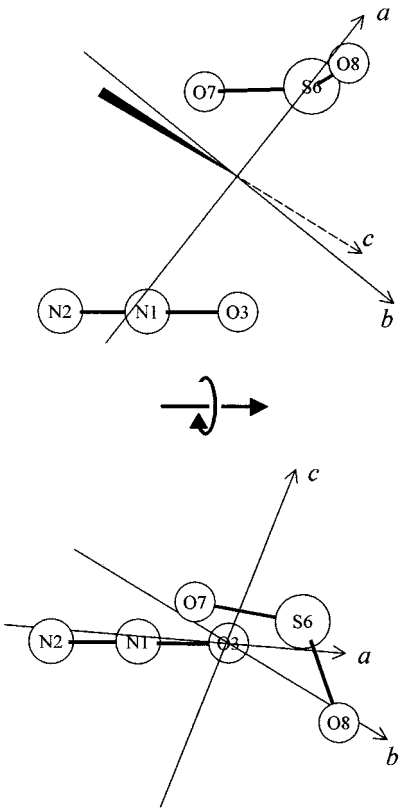

Figure 4. Structure predicted by a semiempirical model for N_2O-SO_2. See Figure 3 for an explanation of the orientation of the complex.

parameters resulting from the semiempirical calculation are given in the last column of Table 8 for comparison. Since the difference between the experimental structures is much smaller than the difference between experiment and the semiempirical calculations, it is not possible to favor one of the structures based on theoretical arguments. The semiempirical calculations on the SO_2 complexes with CO_2, OCS, and CS_2 also did not agree well with experiment in quantitative details.

Discussion

A. Structure Inferences. The most unambiguous conclusion is that $N_2O{\cdot}SO_2$ lacks a plane of symmetry. Its structure resembles the SO_2 complexes with CO_2, OCS, and CS_2 with the SO_2 straddling the N_2O axis but in an asymmetric fashion in this case. Whether the equilibrium structure is closer to structures I−IV where the asymmetry is slight or the more asymmetric ORIENT structure (Figure 4) cannot be clearly ascertained from the data and level of calculations presented here. The isotopic data available in this study is normally sufficient to determine reasonably reliable quantitative parameters, but the poor agreement for the Kraitchman substitution coordinates and the dipole moment projections with the four fitted structures cautions against accepting any of them too literally. Perturbations in the moments of inertia from the tunneling motion are at the core of the problem. Calculating corrections to the moments due to this large-amplitude motion is beyond the scope of this study, as are high-quality semiempirical or ab initio modeling of $N_2O{\cdot}SO_2$. The latter is likely to be the most productive way to advance the understanding of this system at the present time.

B. Structure Comparisons. Comparison of the structural parameters of N_2O-SO_2 with those for the three similar molecules previously studied leads to some interesting observations. The most obvious of these is the lack of symmetry in the N_2O complex. The fact that the complex is isoelectronic with CO_2 leads one to expect a structure with C_s symmetry, since the lack of symmetry in the N_2O monomer makes the C_{2v} arrangement observed for CO_2-SO_2 unlikely. The twisted structure of N_2O-SO_2 makes a comparison of intermolecular distances more meaningful than a comparison of angles. The R_{cm} distance in CO_2-SO_2 is 3.29 Å, while in N_2O-SO_2 it is about 3.33 Å. This distance and some other atom−atom distances are apparently similar.

The twisting of SO_2 is consistent with the differences seen between $CO_2{\cdot}HCCH$[7] and $N_2O{\cdot}HCCH$[8] and between $CO_2{\cdot}H_2O$[4] and $N_2O{\cdot}H_2O$.[5,6] Both of the CO_2 complexes have a symmetric planar structure with the center of the second molecule in line with the carbon of the CO_2. In $CO_2{\cdot}HCCH$ the monomers are parallel, and in $CO_2{\cdot}H_2O$ the hydrogen atoms point away from CO_2 giving a roughly T-shaped geometry. In the N_2O complexes, however, one hydrogen atom from the acetylene or water molecule tilts toward the oxygen of the N_2O. This leads to a nonparallel structure for $N_2O-HCCH$ and a distorted T-shaped structure for N_2O-H_2O. The asymmetric structure in $N_2O{\cdot}SO_2$, when compared to CO_2-SO_2, shows perhaps more drastic changes than observed in the other CO_2 and N_2O systems discussed. Aside from the twisting away from C_s symmetry it is quite similar to the structure observed for $OCS-SO_2$. It is also possible that the observed C_{2v} configuration for CO_2-SO_2 is the average structure and that the equilibrium structure has the C_s symmetry predicted by the ORIENT program with a small barrier at the C_{2v} form.[2]

A comparison between the CO_2-SO_2 and N_2O-SO_2 structures predicted by the ORIENT semiempirical model shows less dramatic, though large, differences. Since the global minimum structure for CO_2-SO_2 has C_s symmetry, only a relatively small twist of the SO_2 is required to get from the CO_2 to the N_2O structure. The C−S distance obtained from ORIENT is 3.69 Å compared to a 3.64 Å distance in the N_2O-SO_2 prediction, emphasizing the similarity between the complexes. It is important to note, however, that the calculations on CO_2-SO_2 employed an adjusted value of the preexponential factor K which led to good reproduction of the C−S distance in the C_{2v} structure. The default value of K was used for the N_2O-SO_2 calculations, so the distances may not be strictly comparable. The experimental N−S distance in N_2O-SO_2 is 3.69 Å (structure I), showing an impressive agreement with the ORIENT calculation. The experimental R_{cm} distance is 3.33 Å though, compared to a model distance of 3.62 Å. It is interesting that the semiempirical model has reproduced one distance well while differing by nearly 0.3 Å in the other. It appears upon examination of the two structures that this is due to a tipping of the SO_2 plane downward (toward N1) in the experimental structure while leaving the sulfur atom in roughly the same position as predicted by ORIENT.

The diversity of structural forms for dimers of SO_2 can be further extended to its dimers with other linear molecules such as HCCH,[20,21] HF,[22,23] HCl,[22] N_2,[24] and HCN,[25] illustrated in Figure 5. It is apparent that the delicate competition between attractive forces (electrostatic, dispersion, polarization) and repulsive forces is subtle and complex. SO_2 is a delicate probe of these interactions. These are challenging systems to model, and certainly an interesting set to test state-of-the-art calculations.

Summary

The structure of the N_2O-SO_2 dimer is asymmetric, unlike the structure of the similar complexes, CO_2-SO_2, $OCS-SO_2$,

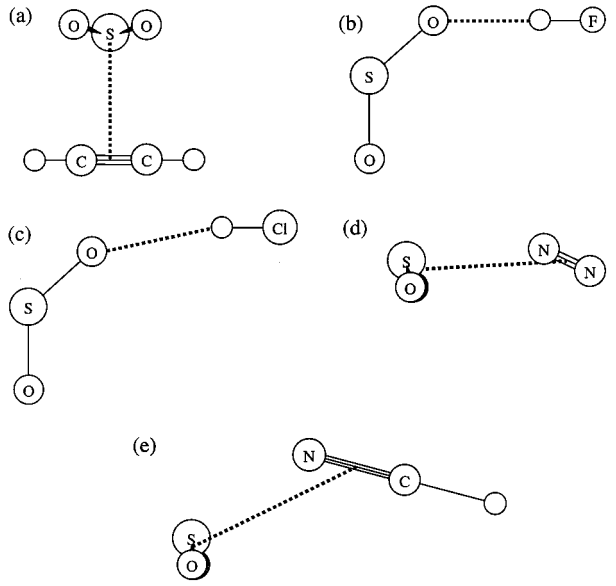

Figure 5. Dimers of SO_2 with linear molecules: (a) $HCCH-SO_2$, (b) $HF-SO_2$, (c) $HCl-SO_2$, (d) N_2-SO_2, (e) $HCN-SO_2$. See text for references.

and CS_2-SO_2. A tunneling motion is present in the complex. The asymmetry of the structure indicates that the motion involved is equivalent to moving the SO_2 through a C_s structure to a mirror image conformation, similar to that observed for $OCS-SO_2$. The fit of the structural parameters to moments of inertia of the isotopic species gives four possible structures for the complex. Dipole moment arguments, the quality of the fits, and comparison with Kraitchman coordinates are inconclusive in identifying a clear preference among the four fitted structures. Comparison with other complexes in the series is not straightforward due to the asymmetry, but R_{cm} and atom−atom distances are similar in going from CO_2-SO_2 to the isoelectronic N_2O-SO_2. Comparison of the structures predicted with a semiempirical model led to a difference of only 0.05 Å in the C−S and N−S distances. Agreement between the semiempirical model and experiment was equally good for the N−S distance, but the rotation of the SO_2 away from a C_s structure was much greater than suggested by the experimental data, and the center of mass distances differed by about 0.3 Å. It seems that the ORIENT model is able to predict qualitatively the structures of dimers of SO_2 with linear molecules in most cases, but further refinement will be necessary to obtain quantitative results. It will be interesting to see how well the model behaves when predicting trimers involving SO_2 and linear molecules, and work in this area is in progress.

Acknowledgment. The authors thank the National Science Foundation, Experimental Physical Chemistry Program, for funding this research and Dr. Sean Peebles for useful discussions on many aspects of the work. R.A.P. thanks the Alfred P. Sloan Foundation and the University of Michigan Center for the Education of Women for a fellowship which supported this research.

References and Notes

(1) Sun, L. H.; Ioannou, I. I; Kuczkowski, R. L. *Mol. Phys.* **1996**, *88*, 255.

(2) Peebles, S. A.; Sun, L. H.; Ioannou, I. I.; Kuczkowski, R. L. *J. Mol. Struct.* **1999**, *485*−*486*, 211.

(3) Peebles, S. A.; Sun, L. H.; Kuczkowski, R. L. *J. Chem. Phys.* **1999**, *110*, 6804.

(4) Block, P. A.; Marshal, M. D.; Pedersen, L. G.; Miller, R. E. *J. Chem. Phys.* **1992**, *96*, 7321.

(5) Peterson, K. I.; Klemperer, W. *J. Chem. Phys.* **1984**, *80*, 2439.

(6) Zolandz, D.; Yaron, D.; Peterson, K. I.; Klemperer, W. *J. Chem. Phys.* **1992**, *97*, 2861.

(7) Muenter, J. S. *J. Chem. Phys.* **1989**, *90*, 4048.

(8) Peebles, R. A.; Peebles, S. A.; Kuczkowski, R. L.; Leung, H. O. *J. Phys. Chem. A* **1999**, *103*, 10813.

(9) Balle, T. J.; Flygare, W. H. *Rev. Sci. Instrum.* **1981**, *52*, 33.

(10) Hillig, K. W., II; Matos, J.; Scioly, A.; Kuczkowski, R. L. *Chem. Phys. Lett.* **1987**, *133*, 359.

(11) Grabow, J.-U. Ph.D. Thesis, University of Kiel, Kiel, 1992.

(12) Muenter, J. S. *J. Chem. Phys.* **1968**, *48*, 4544.

(13) Harmony, M. D.; Laurie, V. W.; Kuczkowski, R. L.; Schwendeman, R. H.; Ramsay, D. A.; Lovas, F. J.; Lafferty, W. J.; Maki, A. G. *J. Phys. Chem. Ref. Data* **1979**, *8*, 619.

(14) Wilson, E. B.; Decius, J. C.; Cross, P. C. *Molecular Vibrations*; McGraw-Hill: New York, 1955.

(15) Kraitchman, J. *Am. J. Phys.* **1953**, *21*, 17.

(16) Stone, A. J.; Dullweber, A.; Hodges, M. P.; Popelier, P. L. A.; Wales, D. J. *ORIENT*: A program for studying interactions between molecules, Version 3.2; University of Cambridge, 1995.

(17) Stone, A. J. *The Theory of Intermolecular Forces*; Clarendon Press: Oxford, UK, 1996.

(18) *CADPAC*: The Cambridge Analytic Derivatives Package Issue 6, Cambridge, 1995. A suite of quantum chemistry programs developed by Amos, R. D., with contributions from Alberts, I. L.; Andrews, J. S.; Colwell, S. M.; Handy, N. C.; Jayatilaka, D.; Knowles, P. J.; Kobayashi, R.; Laidig, K. E.; Laming, G.; Lee, A. M.; Maslen, P. E.; Murray, C. W.; Rice, J. E.; Simandiras, E. D.; Stone, A. J.; Su, M.-D.; Tozer, D. J.

(19) Mirsky, K. In *The Determination of Intermolecular Interaction Energy By Empirical Methods*; Schenk, R., Olthof-Hazenkamp, R., Van Koningveld, H., Bassi, G. C., Eds.; Delft University Press: Delft, The Netherlands, 1978.

(20) Muenter, J. S.; DeLeon, R. L.; Tokozeki, A. *Faraday Discuss. Chem. Soc.* **1982**, *73*, 63.

(21) Andrews, A. M.; Hillig, K. W., II; Kuczkowski, R. L.; Legon, A. C.; Howard, N. W. *J. Chem. Phys.* **1991**, *94*, 6947.

(22) Fillery-Travis, A. J.; Legon, A. C. *Chem. Phys. Lett.* **1986**, *123*, 4.

(23) Fillery-Travis, A. J.; Legon, A. C. *J. Chem. Phys.* **1986**, *85*, 3180.

(24) Juang, Y. D.; Walsh, M. A.; Lawin, A. K.; Dyke, T. R. *J. Chem. Phys.* **1992**, *97*, 832.

(25) Goodwin, E. J.; Legon, A. C. *J. Chem. Phys.* **1986**, *85*, 6826.